Engineering Fracture Mechanics 249 (2021) 107754

Contents lists available at ScienceDirect

Engineering Fracture Mechanics

journal homepage: www.elsevier.com/locate/engfracmech

Transition time threshold for Double Cantilever Beam specimens under high loading rates

S.A. Medina *, E.V. González, N. Blanco

AMADE - Analysis and Advanced Materials for Structural Design, Polytechnic School, Universitat de Girona, Carrer de Maria Aurèlia Capmany i Farnés, 61, 17003 Girona, Spain

ARTICLE INFO

Keywords:
Double Cantilever Beam
Fracture toughness
Quasi-static analysis
High loading rates
Dynamic effects

ABSTRACT

Inertial force effects complicate the determination of the mode I interlaminar fracture toughness under high loading rates in composites. Although using a quasi-static analysis is a common approach, it is not always valid. A time-based threshold criterion is proposed to determine when dynamic effects might be neglected during the analysis of a high loading rate Double Cantilever Beam test. The criterion compares a transition time, time after which inertia effects can be neglected, versus the time for the initiation of fracture propagation. Three different methods are considered for the transition time. Good agreement is found when comparing the expressions with numerical simulations. It is also demonstrated that the transition time is affected by the velocity profile. The proposed criterion and approach to determine the transition time are useful tools to define when a quasi-static data-reduction scheme can be used.

1. Introduction

Fibre reinforced composite materials are increasingly used in automotive and aircraft industries because of their high specific performance [1]. When used in crash safety structures, a thorough assessment of the failure is required not only at quasi-static but also at high loading rates. In these cases, one of the most important material properties is the interlaminar fracture toughness for delamination. In the quasi-static regime, the measurement of the mode I fracture toughness is well established by the Double Cantilever Beam (DCB) test and described in several standards, such as the ISO 15024:2001 [2]. At high loading rates, different test configurations and data reduction methods have been proposed [3–6]. Even so, there is no agreement on the trend of fracture toughness nor the most appropriate testing method. This is due, in part, to the complexity in this analysis of the inertial forces and reflected stress waves involved, and their contribution to the kinetic energy of the system [7–9].

The kinetic contribution in dynamic events may be analysed in different scenarios. In the case of rapid loading events, reflecting stress waves influence the local crack-tip stress and strain fields, affecting the initiation or propagation of fracture [10]. In situations where stress waves reflect back to the crack tip, the stress intensity must be determined for each particular case. Kalthoff et al. [11] studied the effect stress waves have on the stress intensity factor at the crack arrest, using internal wedge-loaded DCB specimens. The geometry design of the common DCB specimen is such that stress waves can reach the specimen boundaries and return back to the crack tip in a very short time. Thus, if the fracture event takes place after the elastic waves have made several reflections within the specimen length, the stress wave effect might be ignored and static equilibrium can be assumed.

When the structure is loaded in short-time, but the stress wave effect can be ignored, inertia effects can be relevant due to accelerations in the system. The load tends to increase with time, but oscillates at a particular frequency, which depends on the

* Corresponding author.
E-mail address: sergio.medina@udg.edu (S.A. Medina).

https://doi.org/10.1016/j.engfracmech.2021.107754
Received 17 December 2020; Received in revised form 9 March 2021; Accepted 16 April 2021
Available online 5 May 2021

Nomenclature

a	DCB and SENB crack length
a_o	DCB initial crack length
b	DCB specimen width
B	SENB specimen thickness
C	DCB specimen compliance
c_o	Sound propagation velocity in the material
C_s	SENB specimen compliance
D	Dimensionless displacement coefficient
E	Young's moduli of the material
E_1, E_2, E_3	Young's moduli of the material
G_{Ic}, G_{IIc}	Interface fracture toughness
G_{12}, G_{13}, G_{23}	Shear moduli of the material
h	DCB specimen thickness of one arm
H	SENB specimen width
$k^{dyn}(t)$	Böhme dynamic correction function
$K_I^{dyn}(t)$	Dynamic stress intensity factor
$K_I^{qs}(t)$	Quasi-static stress intensity factor
l	DCB specimen length
L	Half of the spean between SENB specimen supports
t	Time
t_c	Threshold time
t_f	Time to fracture
t_τ	Transition time
t_{τ_B}	Böhme transition time
t_{τ_I}	Ireland transition time
t_{τ_N}	Nakamura et al. transition time
$u(x)$	DCB opening displacement
$\dot{u}(x)$	DCB displacement rate
U_e	Elastic energy
U_k	Kinetic energy
α	Coefficient for the ratio of threshold time and transition time
β	Coefficient of a power law
δ	DCB opening displacement at the loading point
$\dot{\delta}$	DCB opening rate at the load-line
η	Mixed-mode fit parameter
γ	Power coefficient of a power law
λ_n	Coefficients of the function ξ
ν_{12}, ν_{13}, ν_{23}	Poisson's ratios of the material
ψ	Polynomial function for the effects of D
ρ	Density of the material
τ_I, τ_{II}	Interface strength of the material
ξ	Correlation function for the general expression of energy ratio

Acronyms

3PB	Three-Point Bend
C3D8I	Solid element with incompatible modes
CFRP	Carbon Fibre Reinforced Polymer
COH3D8	Zero-thickness cohesive element
DCB	Double Cantilever Beam
FE	Finite Element
FPZ	Fracture Process Zone
QS	Quasi-static
SENB	Single Edge Notched Bend

specimen material and geometry. The amplitude of these oscillations decreases with time, as kinetic energy is damped by the specimen material. In the cases where a dynamic analysis is required, different approaches may be used such as the one proposed by Chen et al. [12,13] that performs a mode I DCB analysis using a dynamics and vibration analysis of Euler–Bernoulli beams.

For sufficiently long-time loading events, where the behaviour is essentially quasi-static, the inertia effects are minimal [10]. Therefore, in these cases the quasi-static approach is valid. To assess the inertia effects in a dynamic test, Nakamura et al. [14,15] defined a time criterion that provides an estimate when inertia effects can be neglected in a Three-Point Bend (3PB) metallic specimen. The criterion uses a transition time, defined as the time when the kinetic energy equals the internal energy, which represents the period where inertia effects are still present in the system. This time is compared against the time for the initiation of fracture propagation (or time to fracture), ensuring that the fracture event takes place at a longer time than the transition time. In that way, a quasi-static analysis can be used to calculate the fracture toughness at a given high loading rate.

The transition time concept was firstly introduced in bending and impact tests for metals (Three-Point Bend test [16], Four-Point Bend test [17] and Charpy V-Notch test [18]). Ireland [19] and Böhme [20] proposed an experimental approach to determine the transition time, whereas Nakamura et al. [14,15] defined it based on numerical studies. To the authors' best knowledge, the transition time has only been used for composite materials by McCarroll [21], and it was taken into account to justify the use of quasi-static models for the determination of the translaminar mode I fracture toughness in a compact tension specimen. Blackman et al. [8] proposed a criterion to define when a quasi-static or a dynamic approach might be used for the analysis of a pure mode I DCB test carried out under high loading rates.

The present work reformulates the transition time defined by Nakamura et al. [14,15] and defines a time-based threshold criterion to characterise the pure mode I interlaminar fracture toughness under high loading rates in composite materials using the DCB test. Using a geometrical scalability analysis with three different materials, this study assesses the different methods proposed to obtain the transition time. In addition, the influence of the velocity profile and its maximum value over the transition time are analysed. The approach is validated through a numerical analysis implemented as a three-dimensional dynamic Finite Element (FE) model.

2. Theoretical background of the transition time

In this section three different models available in the literature for the determination of the transition time (t_τ) are summarised. For all three cases, the aim is to determine a characteristic time after which inertia effects can be neglected and a dynamic event can be accurately described by means of a quasi-static model.

Nakamura et al. [14] defined a transition time (t_{τ_N}) as the time at which the kinetic energy and the internal energy are equal in a high loading rate test. However, measuring kinetic and internal energies separately during a fracture mechanics test is a difficult task. For this reason, Nakamura et al. proposed to estimate the kinetic energy and the elastic energy through an analytical model based on the Euler–Bernoulli beam theory. In order to use this approach, it is necessary to measure the opening displacement and its rate at the loading point. The resulting equation to determine the transition time (t_{τ_N}) for a Single Edge Notched Bend (SENB) steel specimen in a 3PB impact test is:

$$t_{\tau_N} = DS\frac{H}{c_o} \tag{1}$$

$$S = \left(\frac{LBEC_s}{H}\right)^{1/2} \tag{2}$$

where c_o is the sound speed in the material, E is the material Young's modulus, C_s is the specimen compliance that accounts for the crack length, H is the specimen width, B is the thickness and L is half of the span between supports. D is a dimensionless coefficient that depends on the velocity profile during the test (see Section 4).

Ireland [19] analysed the transition time for a 3PB Charpy impact test on metallic specimens for a wide range of cases: from a rapid loading response (dominated by stress waves) to a long-time loading response (dominated by the fundamental structural elastic deformation mode). Ireland introduced the transition time (t_{τ_I}) as an effective specimen inertial oscillation period and cited numerous experimental data to show that inertial effects are dominant for loading times smaller than $2t_{\tau_I}$. The empirical expression can be expressed in the form:

$$t_{\tau_I} = \left(1.68\sqrt{2}\right) S\frac{H}{c_o} \tag{3}$$

Despite being an empirical model, the criterion proposed by Ireland has been widely accepted for the analysis of the dynamic response of 3PB fracture toughness tests using Charpy and drop-weight impact [22,23], and Hopkinson pressure bar apparatus [24]. Jiang and Vecchio [6] explained how Eq. (3) can be derived based on the inertial modelling of a classic Charpy impact test in terms of the natural frequency of the testing system (Charpy impact machine + bending specimen system), obtaining similar results.

Böhme [20] proposed a transition time t_{τ_B} to quantify the dynamic effects in impact tests with SENB specimens. The transition time was obtained based on the definition of a time-dependent function, identified as dynamic correction function $k^{dyn}(t)$. This function is defined as the ratio between the dynamic stress intensity factor $K_I^{dyn}(t)$ (Böhme measured it experimentally using the optical method of caustics) and the quasi-static stress intensity factor $K_I^{qs}(t)$ (analytically calculated). The transition time was defined as the time from which the variation of the dynamic correction function $k^{dyn}(t)$ differs from 1 (the quasi-static value) by less than 10%. The expression for a 3PB specimen in an impact test can be expressed as follows:

$$t_{\tau_B} = k^{dyn}(t)\frac{H}{c_o} \qquad \text{for} \qquad 0.9 \leqslant k^{dyn}(t) \leqslant 1.1 \tag{4}$$

Sunny et al. [25], Shazly et al. [26], Martins et al. [27], and Jones and Davies [28] applied the expression in Eq. (1) from Nakamura's approach to determine the transition time in standard ASTM E23-18 [29] SENB specimens, obtaining that $t_{\tau_N} = 23.3H/c_o$ when the ratio between the crack length and the specimen width is $a/H = 0.5$.

On the other hand, other authors such as Henschel and Krüger [30], used similar approaches to obtain the transition time in a four-point split Hopkinson bending test. However, Eq. (1) depends on geometric parameters that are not always clearly specified or that cannot be directly translated from a ASTM E23-18 specimen to another type of test, leading to incorrect results. Besides, Koppenhoefer and Dodds [31], and Takashima and Minami [32] reported a dependency of the transition time on the loading velocity for Charpy specimens that was not considered by Nakamura et al. [14,15]. Consequently, further analysis is required to generalise the determination of the transition time for different types of tests, including DCB, and test conditions.

3. Definition of the time-based threshold criterion

The models reviewed in the previous section aim at establishing a criterion to determine when a quasi-static-based data reduction method can be used to calculate the fracture toughness under high loading rates. In order to neglect the inertia effects, the criterion defines a limit between a rapid loading (dominated by discrete elastic waves and inertia effects), and a long-time loading (dominated by the elastic energy). Basically, it needs to be ensured that the time when the fracture starts to propagate, referred as time to fracture t_f, is well after the transition time so the response of the system is dominated by the fundamental structural elastic deformation. The criteria proposed by the previously mentioned authors can be summarised as (see Nakamura et al. [14], Ireland [19] and Böhme [20]):

$$\begin{aligned} t_f &> 2t_{\tau_N} \\ t_f &> 3t_{\tau_I} \\ t_f &> t_{\tau_B} \end{aligned} \tag{5}$$

Böhme [20] compared the transition time of the three different methods for the same particular case. From this, it can be considered that the transition time proposed by Böhme is about two times the one considered by Nakamura et al. Thus, these two criteria can be taken as equivalent. On the other hand, as the transition time suggested by Ireland is almost coincident to that proposed by Nakamura et al. the time to fracture according to Ireland's criterion should be 1.5 times higher. Additionally, Ireland's criterion is the most conservative because it quantifies the hammerload oscillations (dynamic effects at the impacting hammer), instead of the dynamic effects at the crack tip as Nakamura et al. and Bömhe. Following Ireland's approach, Dutton and Mines [33] modified the criterion to be used in a Hopkinson bar loaded fracture test as $t_f > 1.1t_{\tau_I}$.

Based on the analysis done by Nakamura et al. [14] and Böhme [20], in the present work a time-based threshold criterion is defined to calculate the mode I fracture toughness under high loading rates for a DCB test [2]. As in the previous analyses, the contribution of the kinetic energy can be considered as minimal when t_f is certain times larger than t_τ. In this work, it is considered that the dynamic effects on the initiation of fracture propagation can be neglected once the ratio of kinetic energy to elastic energy (U_k/U_e) is below 20%. Thus, for times to fracture t_f larger than a threshold time t_c at which the ratio between energies is below 20%, it can be considered that the dynamic event is close to a quasi-static event and a quasi-static data reduction method can be used. This energy threshold is less conservative than other from literature [34], but giving sufficient margin to neglect the dynamic effects. Even so, the user may define a different percentage of energy ratio lower than the 20% to have more conservative analysis. The criterion proposed is formulated in Eq. (6), where the threshold time t_c is expressed in function of the transition time.

$$t_f > t_c = \alpha t_\tau \tag{6}$$

The objective of the present work is not only to assess the value of the coefficient α and the threshold time, but also to clearly determine the time to fracture for different configurations of the DCB test and different loading velocity conditions, ensuring that the dynamic effects on the fracture event are minimal. The time to fracture is obtained through FE simulations. Regarding the transition time, three different approaches are considered to determine it, allowing sound determination of the coefficient α and the threshold time. The three approaches are based on the assumption of the transition time as the time when $U_k/U_e = 1$, as assumed by Nakamura et al. [14]. The first approach consists on an analytical analysis of the energies. The second approach is based on the deduction of a numerically-based expression using the Buckingham Pi theorem [35] and FE simulations. In the third approach, the transition time is determined analysing the evolution of the energy ratio versus a dimensionless time parameter based on FE simulations.

4. Analytical determination of the transition time t_τ

Considering the DCB specimen shown in Fig. 1, the kinetic energy generated during the test can be obtained by integrating one half of the product of the mass by the displacement rate $\dot{u}(x)$ over the initial crack length a_o. Assuming a symmetric opening of the arms, the kinetic energy for the whole specimen is:

$$U_k = 2\left(\frac{1}{2}\rho bh\int_0^a [\dot{u}(x)]^2\,dx\right) \tag{7}$$

where the mass is defined in terms of the density ρ, the specimen width b and the thickness h of one specimen arm, and a is the crack length, which is equal to a_o before the crack starts to propagate.

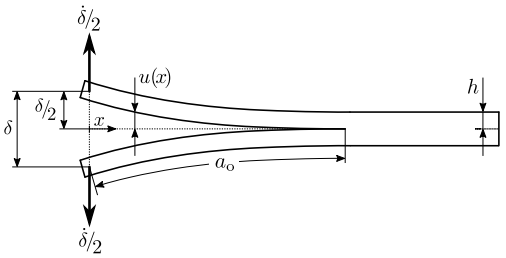

Fig. 1. DCB analysis parameters.

According to the Euler–Bernoulli beam theory and considering no crack propagation, the opening displacement $u(x)$ can be obtained as a function of the opening displacement at the loading point of a single arm ($\delta/2$):

$$u(x) = \frac{\delta}{2}\left(1 - \frac{3x}{2a_o} + \frac{x^3}{2{a_o}^3}\right) \tag{8}$$

Deriving Eq. (8) and replacing in Eq. (7), the kinetic energy in a DCB test can be expressed as:

$$U_k = \frac{33}{560}\rho b h a_o \dot{\delta}^2 \tag{9}$$

where $\dot{\delta}$ is the applied load-line opening rate. This result coincides with the kinetic energy proposed by Hug et al. [36].

On the other hand, the elastic energy of the specimen under bending can be defined in terms of the opening displacement δ and the specimen compliance C as:

$$U_e = \frac{1}{2}\frac{\delta^2}{C} \tag{10}$$

Using the Euler–Bernoulli beam theory, the previous equation can be rewritten as:

$$U_e = \frac{E b h^3 \delta^2}{16{a_o}^3} \tag{11}$$

Eqs. (7) to (11) are equivalent to the ones proposed by Blackman et al. [37]. Then, using the longitudinal wave propagation velocity in the specimen $c_o = (E/\rho)^{1/2}$, the energy ratio from Eqs. (9) and (11) can be expressed as:

$$\frac{U_k}{U_e} = \frac{33}{35}\frac{{a_o}^4 \dot{\delta}^2}{c_o^2 h^2 \delta^2} \tag{12}$$

In order to obtain an explicit expression for the transition time t_τ, it is convenient to introduce the dimensionless displacement coefficient D defined by Nakamura et al. [14] as:

$$D = \left.\frac{t\dot{\delta}}{\delta}\right|_{t_\tau} \tag{13}$$

$$\frac{\dot{\delta}}{\delta} = \frac{D}{t_\tau} \tag{14}$$

Combining Eqs. (12) and (14), the transition time can be expressed as:

$$t_\tau = \left(\frac{33D^2}{35}\frac{{a_o}^4}{{c_o}^2 h^2}\right)^{0.5} = \left(\frac{33D^2}{35}\right)^{0.5}\frac{{a_o}^2}{c_o h} \tag{15}$$

If the displacement is expressed as a power law such as $\delta = \beta t^\gamma$, the value of the parameter D is equal to the power γ. When applying a constant velocity, i.e., step acceleration, D is equal to one. For a linear increment of velocity respect to time, i.e., linear acceleration, D is equal to two.

5. FE analysis of the DCB

In this section two different methods are presented to determine the transition time in a DCB test, a numerically-based method and a graphical method. The FE model used in the simulations to numerically determine and validate the transition time is presented next. At an initial stage, the model is used for the determination of a numerically-based expression of the transition time t_τ using the Buckingham Pi theorem in a dimensional analysis. Then, a geometrical scalability analysis using different materials is performed for the validation of the graphical method.

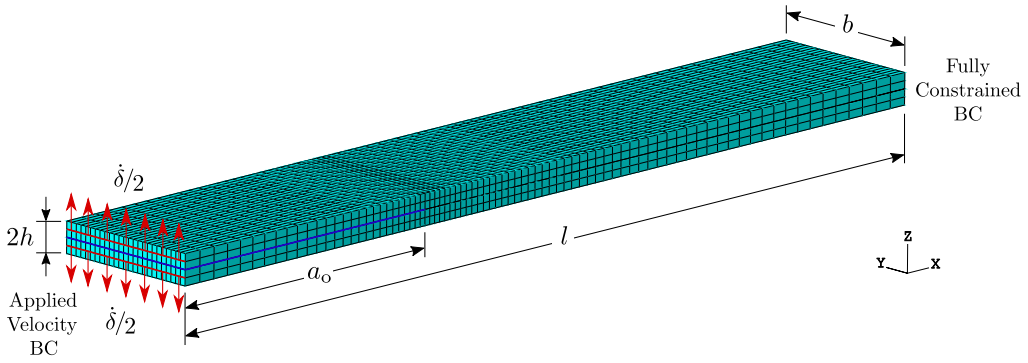

Fig. 2. Geometry, mesh and boundary conditions considered for the numerical analysis of the DCB test.

5.1. FE model description

A three-dimensional model of the DCB specimen is defined using the commercial software Abaqus/Explicit [34]. Solid elements with incompatible modes (C3D8I) are used to capture the bending response due to large displacements, avoiding the shear-locking and hourglass phenomena. Since the studies focus on the global bending behaviour and not on the stress distribution in the material, only two elements in the through-the-thickness direction are used for each of the arms of the specimen. As only the initial stage of loading is considered and the crack propagation is ruled out (constant a_o), the initial pre-crack is modelled merging nodes of the two arms ahead of the crack tip.

One of the main problems of using the classical DCB test under high loading rates is that the specimen deforms unsymmetrically when the load is applied to one of the arms while the other one is fixed to the test rig [7,9]. In order to simulate the ideal situation with symmetrical opening, a prescribed velocity is applied to each of the specimen arms while all the displacements at the other end are constrained. To reduce the computational time of the simulations, the specimen is meshed with regular hexahedral elements using different mesh densities along its length. Near the crack tip a refined mesh is used with an element size of 1 mm, while away from the crack tip, a coarse mesh with an element size of 3 mm is employed. A progressive mesh is defined in between. The width of the elements is set to 1 mm in all areas. The boundary conditions and meshing of the model are shown in Fig. 2.

5.2. Numerically-based determination of the transition time t_τ

A dimensionless framework based on the Buckingham Pi theorem [35] combined with an inverse analysis is used for the numerical determination of the transition time. The use of FE simulations allows to obtain an accurate transition time that accounts for the effects neglected in the approach reported in Section 4. Moreover, the dimensionless framework allows studying the scalability of results between different geometries and/or materials in DCB specimens.

The dimensional analysis relies on the proper selection of the variables that influence the problem. For the determination of the transition time, the ratio between the kinetic and elastic energies can be expressed as a function of all the involved variables as:

$$\frac{U_k}{U_e} = f\left(t, \delta, \dot{\delta}, c_o, a_o, h, b, l\right) \tag{16}$$

where the energy ratio U_k/U_e is the dependent variable. The variable t is the time of the test, δ is the displacement and $\dot{\delta}$ is the maximum applied velocity (applied loading rate). The variable c_o is the sound propagation velocity. The geometrical parameters of the specimen are the initial crack length a_o, the thickness of one arm h, the width b and the length l.

Taking into account that not all the variables affect the problem in the same way, a preliminary analysis is carried out to assess the effect of the overall variables over the problem, and reduce these variables using the Buckingham Pi theorem (see Appendix A). After the results of the preliminary analysis, the length and the width have no effect on the energy ratio. Therefore, these variables can be removed for the dimensional analysis. Another change with respect to the preliminary dimensional analysis is that as indicated in Appendix A, it is better to use a_o as a repeating variable instead of δ. Therefore, the repeating variables for this analysis are t and a_o. With the change of the repeating variables, the dimensionless displacement coefficient D defined by Nakamura et al. [14] is not longer obtained. However, it is possible to introduce it as a combination of two π-parameters: $t\dot{\delta}/a_o$ and a_o/δ. This allows to simplify the analysis in one π-parameter less and consider the coefficient D in order to analyse the effect of the applied velocity (see Sections 7.2 and 7.3). Thus, according to the Buckingham Pi theorem [35], the energy ratio can be defined as a function of three π-parameters:

$$\frac{U_k}{U_e} = f\left(\pi_1 = \frac{tc_o}{a_o}, \pi_2 = D = \frac{t\dot{\delta}}{\delta}, \pi_3 = \frac{h}{a_o}\right) \tag{17}$$

To obtain the function that describes the relation from Eq. (17), a parametric study using FE simulations is carried out. In this study, the effect of each π-parameter over the energy ratio is assessed in such a way that while one π-parameter is varied, the

Table 1
Values for the dimensionless π-parameters for the scalability analysis.

$\frac{U_k}{U_e}$	$\frac{tc_o}{a_o}$	$D = \frac{t\dot{\delta}}{\delta}$	$\frac{h}{a_o}$	$\frac{b}{a_o}$	$\frac{l}{a_o}$
Response variable	Response variable	1 and 2	0.05	0.5	3

other π-parameters remain constant. A curve for each π parameter versus the energy ratio is obtained. In order to obtain these curves, the same approach from the simulations done in Appendix A is used, only changing the repeating variable (a_o). From each π-parameter curve, a fitting expression is obtained by means of a non-linear regression analysis, as summarised in Appendix B. With this procedure, a general expression, Eq. (B.2), describing the variation of the energy ratio in function of the different variables is obtained. However, this expression is too complex and results unpractical. Taking into account that the analysis is focused on the time solution at which the energy ratio is one, the initial evolution of the energy ratio curve may be avoided. Then, a simpler master expression that combines all the π-parameters can be defined to obtain the decreasing part of the energy ratio curve for a DCB specimen as:

$$\frac{U_k}{U_e} = \psi \frac{a_o^{4.402}}{c_o^{2.269}\, h^{2.133}\, t^{2.269}} \tag{18}$$

where ψ is a polynomial function that accounts for the effects of the dimensionless parameter D and it is described in Eq. (19).

$$\psi = -0.3876D^3 + 3.0778D^2 - 4.0069D + 1.8696 \tag{19}$$

Equalling $U_k/U_e = 1$, a new expression for the transition time can be obtained:

$$t_\tau = \left(\psi \frac{a_o^{4.402}}{c_o^{2.269}\, h^{2.133}} \right)^{0.44} = \psi^{0.44} \frac{a_o^{1.937}}{c_o^{0.998}\, h^{0.938}} \tag{20}$$

Comparing Eq. (15), analytical approach, and Eq. (20), numerically-based approach, it can be observed that both equations follow the same pattern but with certain differences in the coefficients affecting D and the exponents affecting a_o, c_o and h. For the case of a step acceleration, $D = 1$, the coefficients for the analytical (taken in front of $a_o^2/c_o h$) and the numerically-based expressions (taken in front of $a_o^{1.937}/c_o^{0.998}h^{0.938}$) are 0.971 and 0.770, respectively. For the case of a linear acceleration, $D = 2$, these coefficients for the analytical and the numerically-based expressions are 1.942 and 1.637, respectively. The indexes of the power for the analytical expression for a_o, c_o and h are 2, 1 and 1, respectively. While for the numerically-based expression are 1.937, 0.998 and 0.938, respectively. Therefore, despite the similitude of the expressions, relatively different predictions of the transition time may be expected with both methods and a further analysis is required to elucidate which of the two is more accurate (see Section 6).

5.3. Graphical determination of the transition time t_τ

A third approach is based on the graphical representation of the evolution of the energy ratio obtained through FE simulation versus time or the dimensionless time parameter tc_o/a_o (for each FE simulation, a_o and c_o remain constant and only t varies). Following the same concept of Nakamura et al. [14], the values of the transition time t_τ or the dimensionless time parameter $t_\tau c_o/a_o$ are obtained when the energy ratio is equal to one ($U_k/U_e = 1$).

This graphical method, as a dimensionless approach using tc_o/a_o, can be used not only for the particular simulation, but also for scalable similar problems. This signifies that the results obtained with this method are not only valid for the case considered but also for any DCB specimen, where the combination of parameters result in the same values of π_2 and π_3, independently of the material or initial crack length. The use of this method is shown in the following section for a geometrical scalability analysis.

5.4. Geometrical scalability analysis for different materials

A parametric FE analysis is carried out to validate the capabilities of the Buckingham Pi theorem approach and the expression for the determination of the transition time proposed in Eq. (20) in terms of geometrical scalability and dynamic similarity.

The parametric study considers a wide range of scenarios, varying the geometrical and material variables while keeping the other π-parameters introduced in Eq. (17) constant, as indicated in Table 1. The resulting energy ratio versus time and the dimensionless time parameter (π_1-parameter) curves allow to illustrate the graphical method proposed in Section 5.3. Although as shown in Section 4 and Appendix A, the length and the width of the specimen do not affect the results, they are defined accordingly to the size of the crack length to maintain the value of the corresponding π-parameters as constant.

All the simulations are carried out considering a maximum velocity of 2 m/s for the applied load. However, two different scenarios are taken into account: (i) step acceleration ($D = 1$) and (ii) linear acceleration ($D = 2$). Three different materials are considered: steel and two different Carbon Fibre Reinforced Polymers (CFRPs), Hexply AS4/8552 and TeXtreme®, whose properties are summarised in Table 2. For each material, three different cases are considered based on the different values of the geometrical

Table 2
Material properties for the scalability analysis.

	ρ [kg/m^3]	E_1 [GPa]	ν_{12}	$c_o = (E/\rho)^{1/2}$ [m/s]
Steel	7850	210.0	0.3	5421.9
AS4/8552 [38]	1590	128.0	0.35	9578.2
TeXtreme® [39]	1500	61.4	0.042	6405.3

Table 3
Values of the geometrical variables for each material configuration in the geometrical scalability analysis.

Geom. variables	Case 1	Case 2	Case 3
a_o [mm]	50	25	70
h [mm]	2.5	1.25	3.5
b [mm]	25	12.5	35
l [mm]	150	75	210

variables. These three cases are reported in Table 3. For each case, the values of the dimensionless π-parameters listed in Table 1 are respected.

During the parametric analysis, the geometry and mesh of the FE model reported in Section 5.1 are adapted to the corresponding configuration. The mesh for Case 1 has 1 mm elements in the refined mesh zone (near the crack tip), while 3 mm mesh size is used in the region away from the crack tip (the opposite ends). The mesh size is scaled up proportionally for Case 2 and Case 3. The kinetic energy U_k and the elastic energy U_e of the specimens are directly obtained from the simulation.

Fig. 3 presents the results of the scalability analysis. The scalability is assessed for each of the three different materials by means of the evolution of the energy ratio. The charts in the left column of Fig. 3 show the energy ratio versus time curves for the three different materials (steel, AS4/8552 and TeXtreme®), the three geometrical cases and the two velocity profiles considered. As it can be observed for each velocity condition, the energy ratio evolution is equal for the three geometrical cases but with a certain time delay or offset. As seen in the figures, the energy ratio increases from zero in an unsteady manner until a maximum value is reached. Further, the energy ratio decreases rapidly below 1, which corresponds to the transition time defined by Nakamura et al. [14,15], and with a global tendency towards 0. It can also be seen that for the same geometrical case, the evolution of the energy ratio is steadier when $D = 2$ but the maximum energy ratio and the transition time occur later.

On the other hand, the charts in the right column of Fig. 3 show the curves of the variation of the energy ratio versus the dimensionless time parameter. It can be observed that for each material and for each velocity condition, the energy ratio profile is the same for the three geometrical cases. Accordingly, one value of $t_\tau c_o/a_o$ determines the transition time for the three different scalable cases. In addition, thanks to the scalability analysis carried out, the obtained transition time is valid for any DCB test, independently of the corresponding material and initial crack length, provided that the values of π_2 and π_3 are the same.

6. Assessment of the proposed methods to determine the transition time

The different methods to determine the transition time can be assessed using the FE simulations of the scalability analysis. First, the evolution of the energy ratio versus time obtained from the FE simulations is plotted versus time, as shown in Fig. 4a for $D = 1$ and Fig. 4b for $D = 2$, which corresponds to the graphical method. It is worth remarking that the results for the three configurations or cases considered in Section 5.4 are very similar. Thus, for conciseness, only the results for Case 1 are represented in Fig. 4. In addition, for the sake of clarity, the figure only presents the time range after which the maximum value of the energy ratio is achieved. Then, the variations of the energy ratio predicted using the analytical (Eq. (12)) and the numerically-based (Eq. (18)) methods are included for comparison. In this way, it is not only possible to assess the accuracy of the analytical and the numerically-based methods in predicting the transition time but also the good approximation in capturing the evolution of the energy ratio.

From Fig. 4, a general agreement is seen between the different methods, particularly around the transition time region ($U_k/U_e = 1$). However, after the transition time, the analytical and numerically-based expressions show a different tendency than the graphical method from the FE simulation, especially for the case with $D = 1$. This might be due to the effect of the infinite acceleration profile at $t = 0$ which cause vibrations in the arms of the specimen adding kinetic energy from the wave propagation and other effects that are not taken into account in Eqs. (12) and (18).

Focusing on the transition time, an assessment of the analytical and numerical expressions, Eq. (15) and (20) respectively, can be done. The obtained transition time values are compared with respect to the values from the graphical method, which can be considered as the reference values, as shown in Table 4.

Analysing the results summarised in Table 4, it can be concluded that there is a good global agreement between the three approaches. The numerically-based approach shows a slightly better accuracy (the maximum difference is of 14.8%), than the analytical method (the maximum difference is of 19.2%). Only in one case (steel and linear acceleration ($D = 2$)) the difference is lower for the analytical approach. On the other hand, the differences are lower for linear acceleration than for step acceleration ($D = 1$), except for the numerically-based approach and steel. The global tendency observed can be explained by the fact that the

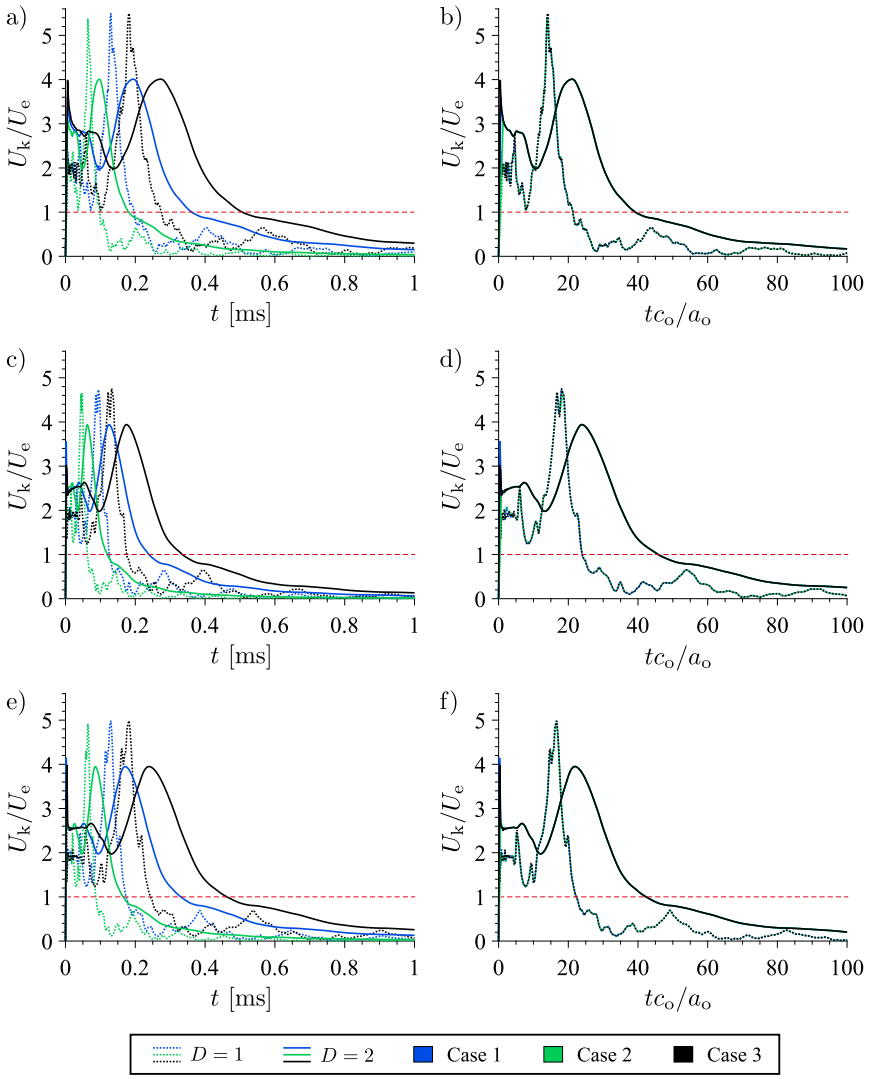

Fig. 3. Variation of the energy ratio versus time (a, c, e) and the dimensionless time parameter (b, d, f). Curves (a) and (b) for steel, curves (c) and (d) for AS4/8552, and curves (e) and (f) for TeXtreme®.

Table 4
Results of the transition time for Case 1 using the graphical approach, the analytical expression and the numerically-based expression, showing the percentage of difference (%DIFR) versus the graphical method. All values of τ are in [ms].

Material	D	Graphic t_τ (FE Sim.)	Analytical t_τ (Eq. (15))	% DIFR	Numerically-based t_τ (Eq. (20))	% DIFR
Steel	1	0.196	0.179	8.7	0.195	0.4
	2	0.362	0.358	1.1	0.415	14.8
AS4/8552	1	0.125	0.101	19.2	0.113	9.9
	2	0.239	0.203	15.1	0.239	0.2
TeXtreme®	1	0.174	0.152	12.6	0.158	9.3
	2	0.330	0.303	8.2	0.336	1.8

analytical method is based on the assumptions of the Euler–Bernoulli beam theory, and the numerically based equation is obtained using non-linear FE simulations. Also a linear acceleration is less abrupt than a step acceleration case, which cannot be so accurately predicted by general approximations. Finally, the numerically-based approach comes from a global fitting of different configurations, losing accuracy in some of the cases but minimising the difference in a global response.

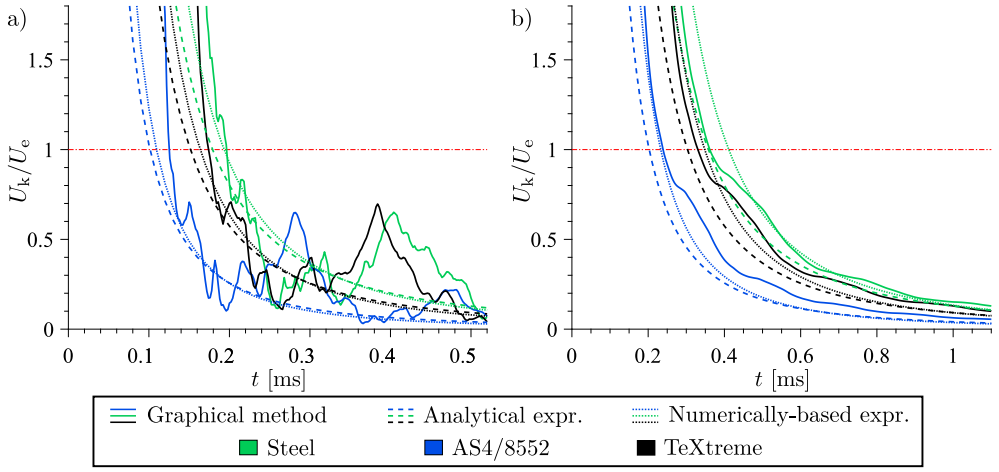

Fig. 4. Comparison of curves of energy ratio for Case 1 from the graphical method, the analytical method and the numerically-based method for (a) step acceleration ($D = 1$) and (b) linear acceleration ($D = 2$).

From the assessment of the different approaches, it is recommended to use the numerically-based method to obtain the transition time. Even so, performing FE simulations to use the graphical method will allow to get not only the transition time but also the general behaviour of the energy ratio.

7. Loading rate effect on the time to fracture

In order to develop the time-based threshold criterion of Eq. (6) for a DCB specimen, in addition to the analysis of the transition time carried out in the previous section, it is also necessary to take into account how the time to fracture behaves. Therefore, in this section, a numerical investigation is carried out to study the effects of the velocity profile and its maximum value on the transition time behaviour in presence of a fracture event, i.e., when the initiation of the crack propagation is considered. The FE model presented in Section 5.1 is used here with some modifications.

7.1. FE model for crack propagation

Since the simulations in this section consider the time for the initiation of crack propagation, t_f, a new numerical model based on the FE model of Section 5.1 is defined. The mesh is refined and zero-thickness cohesive elements COH3D8 are added to capture the onset of delamination. The modelling strategy is described in Fig. 5. The cohesive constitutive behaviour considered is from Abaqus' library, where the onset of delamination is defined by a quadratic stress-based criterion, whereas delamination propagation is characterised by the mixed mode energy-based propagation criterion proposed by Benzeggagh and Kenane [40].

A refined mesh of the model is used to account for the interface delamination with biased transition from coarse mesh to fine mesh (see Fig. 2). The Fracture Process Zone (FPZ) and the element size in the direction of crack propagation are defined based on the approach proposed by Soto et al. [41]. The corresponding length of the FPZ is 1.21 mm and the element size selected around the crack tip is 0.3 mm, thus, ensuring a minimum of three cohesive elements to model the interlaminar FPZ. A maximum size of 0.6 mm is used at the ends of the specimen. An element size of 0.625 mm is defined in the width direction of the whole specimen.

The DCB specimen modelled has an initial crack length of 50 mm, an arm thickness of 1.5 mm, a length of 150 mm, and a width of 25 mm. The material used is Hexply AS4/8552 CFRP composite, with the following elastic properties [38]: $E_1 = 128000$ MPa; $E_2 = E_3 = 7630$ MPa; $G_{12} = G_{13} = 4358$ MPa; $G_{23} = 2631$ MPa; $\nu_{12} = \nu_{13} = 0.35$ and $\nu_{23} = 0.45$. The interface material properties used are [38]: $G_{Ic} = 0.28$ N/mm; $G_{IIc} = 0.79$ N/mm; $\tau_I = 26$ MPa; $\tau_{II} = 78.4$ MPa and $\eta = 1.45$.

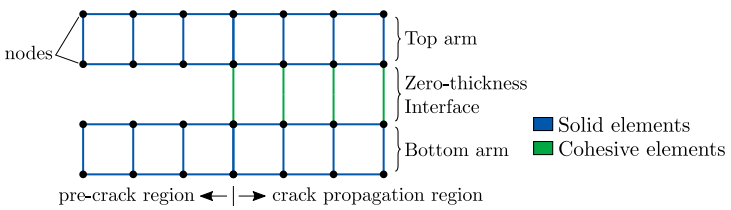

Fig. 5. Sketch of modelling strategy using solid elements with incompatible modes (C3D8I) linked with zero-thickness cohesive elements (COH3D8) to capture the initiation of fracture propagation.

Table 5
Profiles of acceleration for the velocity profile analysis.

Profile	Acceleration value [m/s^2]	Time to constant velocity [ms]
P_1	∞	0 ($D = 1$)
P_2	60×10^3	0.1
P_3	40×10^3	0.15
P_4	20×10^3	0.3
P_5	12×10^3	0.5
P_6	6×10^3	1
P_7	0.33×10^3	1.8 ($D = 2$)

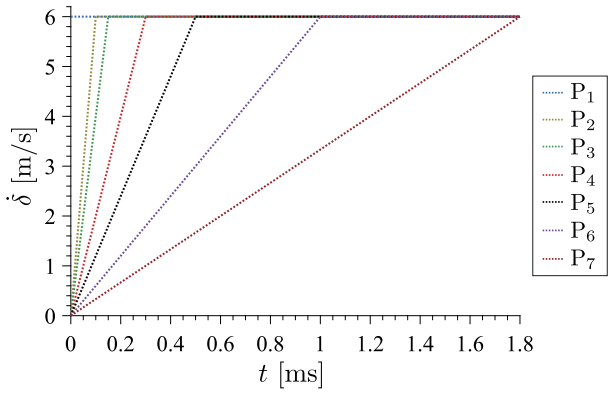

Fig. 6. Velocity profiles of the loading rates response analysis.

7.2. Analysis of the velocity profile

A study of the effect of the velocity profile over the transition time is performed considering different profiles of acceleration, from step acceleration ($D = 1$) to linear acceleration ($D = 2$) for a maximum value of velocity of 6 m/s. The intermediate profiles have a ramp acceleration behaviour, presenting an initial stage of linear acceleration until reaching a state of constant velocity until a final time of 1.8 ms. The description of the different velocity profiles is shown in Table 5 and illustrated in Fig. 6.

Fig. 7 shows the numerical results from the velocity profile analysis. For simplicity and better understanding of the global behaviour around the transition time zone, the initial part of the curves is omitted and, log–log axes are used to represent the evolution of the energy ratio versus the dimensionless time parameter. In the figure, the vertical dashed lines indicate the time when the first row of cohesive elements located at the pre-crack are fully degraded, which can be considered as the t_f. The horizontal lines corresponding to an energy ratio equal to 1 (transition time t_r) and to 0.2 (threshold criterion t_c) are also included in the figure for

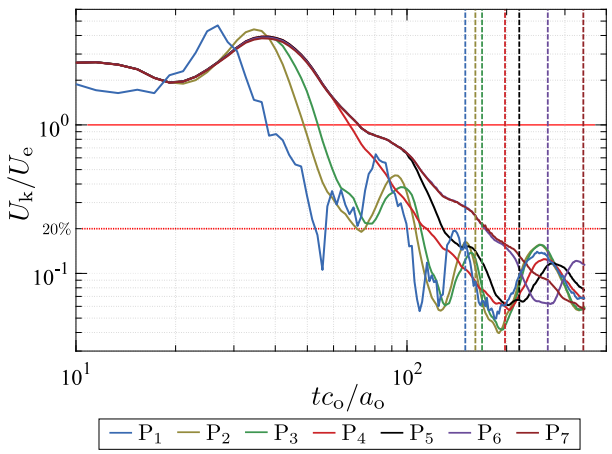

Fig. 7. Variation of the energy ratio versus the dimensionless time parameter for the AS4/8552 composite material with a maximum velocity of 6 m/s and different velocity profiles. The t_f is indicated in each case with vertical dashed lines.

reference. If the 20% energy ratio limit is crossed in several times for a particular case, in general, the threshold time t_c should be taken as the last time when the energy ratio overpasses the defined limit value.

The curves in Fig. 7 show a different response depending on the velocity profile. There is a gradual change in the behaviour of the maximum energy ratio, as well as the waviness of the curves, from profile P_1 to profile P_7. When decreasing the acceleration, both the transition time and the time to fracture increase. This could be reasoned as when the acceleration decreases, a shorter displacement is achieved in a longer time. On the contrary, as D gets closer to one the acceleration is higher, reaching an infinite acceleration when $D = 1$. Additionally, it can be noticed that there is no virtual change in the energy ratio behaviour when moving from profile P_5 to P_7. This means that there is a critical value of acceleration in the velocity profiles below which the energy ratio behaves equal to the case of linear acceleration $D = 2$. Even so, it is worth noting that the relative difference in fracture time from case to case is different to the relative difference in transition time. Still, in all the cases, the fracture time is sufficiently larger than the transition time to consider that for this value of maximum velocity, the effect of the velocity profile can be neglected. This is important for the analysis of the effect of the maximum value of the applied velocity, Section 7.3, and the analysis of the proportionality of the threshold criterion, Section 8. In fact, after the results shown in Fig. 7, it can be considered that the case of linear acceleration, $D = 2$, is representative for a wide range of practical cases and it is only necessary to consider the situations where D is equal to 1 or 2.

7.3. Analysis of the maximum value of velocity

A study of the effect of the maximum value of applied velocity on the transition time is carried out considering a step acceleration ($D = 1$) and a linear acceleration ($D = 2$). Seven maximum velocities (1, 2, 4, 6, 10, 16 and 20 m/s) are considered to get a wide range of loading rates and to determine the limits of using the transition time for a quasi-static analysis in DCB tests. The simulation time is adjusted to reach the initiation of fracture propagation in each case without extending them unnecessarily. The resulting evolutions of the energy ratio for all the considered velocity values when $D = 1$ and $D = 2$ are reported in Fig. 8. Similar to what is observed in Fig. 3, Fig. 8 presents a different pattern in the variation of the energy ratio when D is equal to 1 (Fig. 8a) or when it is equal to 2 (Fig. 8b). In both cases, the energy ratio shows a high amount of kinetic energy at the beginning, in the early load stage. For the step acceleration case, $D = 1$, the curves have a wavy behaviour independent of the velocity applied, even for low energy ratios (below 0.1). If an infinite acceleration is applied to reach the constant velocity, stress waves are generated and propagated through the specimen. Even so, there is a similar tendency in the global behaviour of the curves.

It can be observed in Fig. 8a that the value of the transition time is the same for all the cases except for 16 and 20 m/s, where the propagation of the crack starts before the transition time. For these cases, the variation in the evolution of the energy ratio due to the increase of the internal energy during the crack propagation event, affects the determination of the transition time.

As it can be seen in Fig. 8b, the evolution of the energy ratio is practically the same for all the considered velocities when a linear acceleration is used, $D = 2$. The wavy behaviour is not as prominent as in Fig. 8a since the kinetic energy is becoming less relevant with the evolution of time during the test. The transition time remains practically the same for all the cases since the linear acceleration allows to reach the maximum value of velocity incrementally, and in turn, increasing the kinetic energy progressively.

Although Takashima and Minami [32] demonstrated that for impact velocities higher than 1 m/s (step acceleration assumed), the transition time decreases when increasing the velocity in a Charpy test configuration. However, the current study exhibits that the transition time is practically independent of the maximum value of the applied velocity for a DCB test, as seen in Fig. 8. In fact, the transition time is exactly the same for all the considered values of the maximum velocity when $D = 2$ and it is only different for the two highest values of velocity when $D = 1$, where it may have been affected by the starting of crack propagation.

8. Assessment of the time-based threshold criterion

The transition times obtained in the previous analysis are compared with the time to fracture to determine the proportionality of the time-based threshold criterion of Eq. (6). In all the cases considered in the study of the velocity profile carried out in Section 7.2 for a maximum velocity of 6 m/s (see Fig. 7), the initiation of the fracture propagation takes place when the energy ratio is below 1. In all the profiles the fracture propagation takes place in a time larger than twice the corresponding transition time, fulfilling the time criterion proposed by Nakamura et al. [14,15]. It can be also observed that for all the cases the initiation of the fracture propagation is predicted when the energy ratio is below 20%, in agreement with the limit established in Section 3. However, although the transition time is the same for profiles P_5 to P_7 and almost the same for P_4, the time to fracture in these four cases varies considerably. Even so, imposing that the initiation of fracture propagation must take place once the energy ratio is below 20% ensures that the dynamic effects can be neglected. This is why it is important to carefully assess the transition time and the threshold criterion for each combination of parameters.

Analysing the results of the maximum value of the velocity carried out in Section 7.3, for the case of step acceleration, $D = 1$ (Fig. 8a), it is observed that for values of the maximum velocity equal to 16 and 20 m/s, the time to fracture is lower than the transition time. For the case of a maximum velocity of 10 m/s, the fracture event takes place shortly after the transition time. Therefore, in all these three cases, the time criterion of the fracture time being at least twice the transition time is not fulfilled nor the criterion of an energy ratio below 20%. This implies that for the considered conditions, a quasi-static approach can be used only for velocities below 6 m/s. For a linear acceleration, $D = 2$ (Fig. 8b), the fracture event is reached in all the cases after the transition time, which results to be the same for all. In fact, in all the cases except for a velocity of 20 m/s, the time-based threshold criterion of an energy ratio lower than 20% is assessed. The case of a maximum velocity of 20 m/s is in the limit of the threshold criterion,

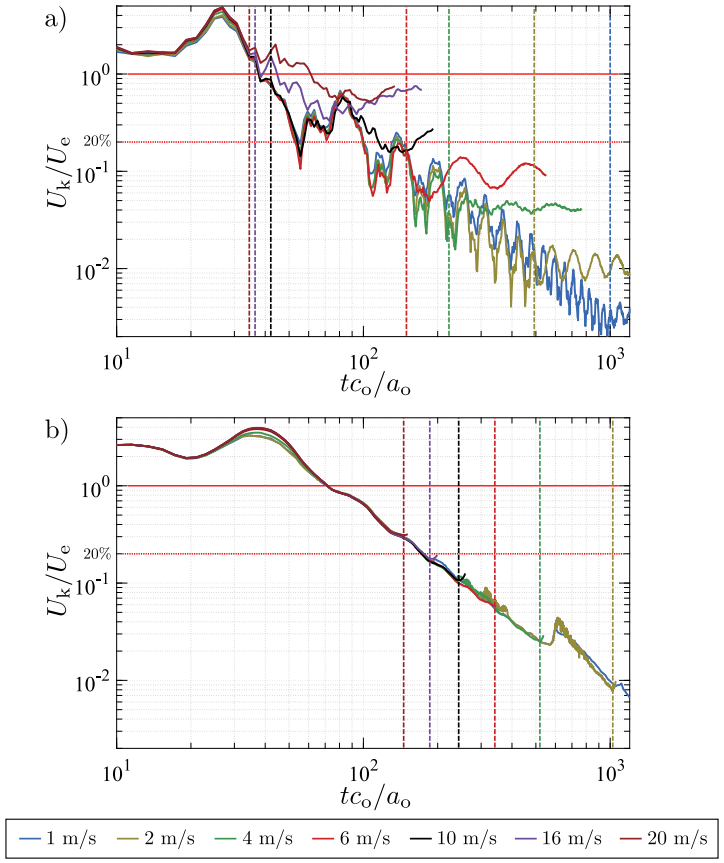

Fig. 8. Variation of the energy ratio versus the dimensionless time parameter with different maximum values of the applied velocity for (a) step acceleration ($D = 1$) and (b) linear acceleration ($D = 2$). The t_f is indicated in each case with vertical dashed lines.

so it is not clear if a quasi-static analysis can be safely used. However, taking into account that the fracture event is predicted for an energy ratio of about 30%, thus above the limit established, dynamic effects cannot be neglected and a dynamic analysis must be considered.

After the analysis of the evolution of the energy ratio for all the cases considered in the previous sections and taking into account the effect of the different parameters on the time to fracture, it can be concluded that to rule out any dynamic effect on the initiation of fracture propagation, the contribution of the kinetic energy should be less than 20%. Additionally, a criterion only based on the proportionality between the time to fracture with respect to the transition time might not be always enough to neglect the contribution of this kinetic energy. Nevertheless, a criterion based on the comparison between the level of energy ratio may be impractical and difficult to implement and assess because of the need of FE simulations to obtain the energy ratio. For this reason, a time-based criterion based on the assumption of an energy ratio below 20% is derived. From Eq. (18) and imposing $U_k/U_e = 0.2$, it is possible to obtain a value for the threshold time t_c through the coefficient α as in Eq. (6). The threshold criterion for the numerically-based approach can be now defined as:

$$t_f > t_c = 2.03 t_\tau \tag{21}$$

After applying and comparing the threshold time criterion proposed by Nakamura et al. [14,15] and the criterion based on the level of the energy ratio proposed in this work on the results of the evolution of the energy ratio of the previous sections (Eq. (21)), it can be concluded that both criteria are almost equivalent. However, the criterion proposed in this work is based on an energies analysis which has a direct relation with the test rather than imposing an arbitrary proportionality of time (in fact, the criterion proposed by Nakamura et al. considers a coefficient between 2 and 3, without further clarification on how to select these values).

In order to summarise the previous discussion, Fig. 9 represents the variation of the transition time and the time to fracture with respect the value of maximum velocity. Fig. 9a corresponds to the case of a step acceleration, while a linear acceleration is considered in Fig. 9b. In both cases, the threshold criterion with $\alpha = 2.03$ in Eq. (21), is included for better visualisation.

It is worth noting that the results in Fig. 9 correspond to the case of a DCB specimen made of unidirectional AS4/8552 carbon epoxy composite with $a_o = 50$ mm, $h = 1.5$ mm, $l = 150$ mm and $b = 25$ mm. Thanks to the scalability analysis carried out, these curves are valid for any DCB specimen made of any possible material provided that h/a_o is equal to 0.03. This makes these results

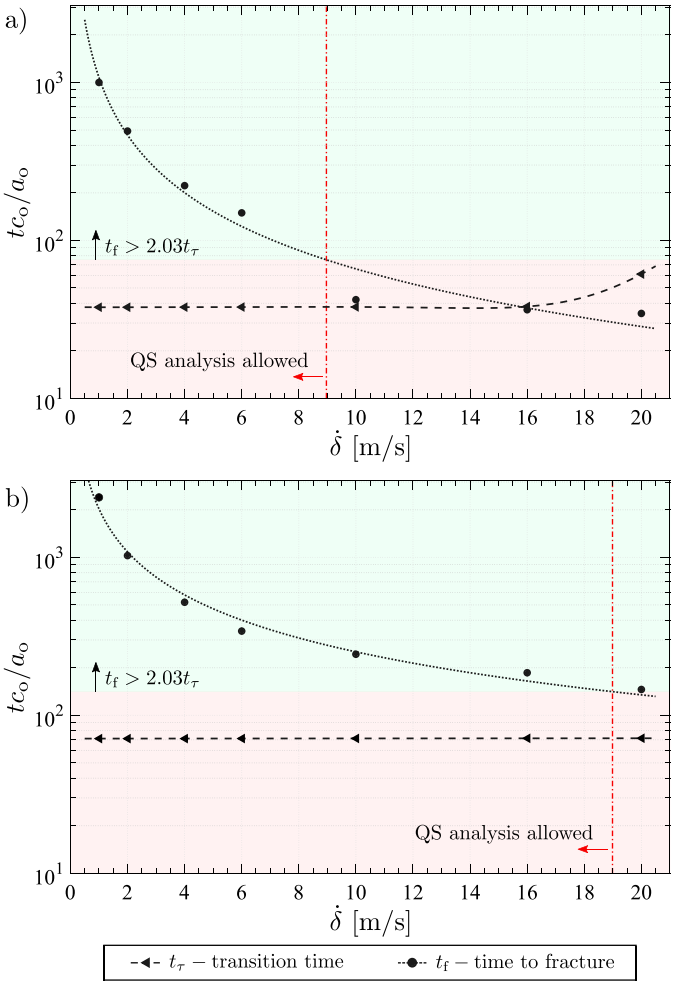

Fig. 9. Dimensionless time parameter for transition time and the time to fracture in a DCB specimen of AS4/8552 composite material versus the maximum value of velocity applied using (a) step acceleration ($D = 1$) and (b) linear acceleration ($D = 2$). The vertical line represents the velocity until which a quasi-static analysis can be performed. The green section represents the cases that fulfil the threshold criterion proposed.

very useful for composite materials because the ASTM D5528-13 [42] standard considers an initial crack length of 50 mm and 3 mm thick specimens.

There are currently few experimental data on dynamic delamination tests available in the literature [5,7,37] that can be used to validate the proposed method. Using the data from the work of Blackman et al. [7,37] for the case of epoxy/carbon-fibre composite at test rates from 0.65 m/s up to 20.50 m/s, applying the numerically-based approach to fulfil the threshold criterion a quasi-static scheme analysis can be safely used for all the test rates. Although in their work Blackman et al. applied the dynamic analysis approach they proposed, they verified that at 8 m/s the contribution of the kinetic energy is negligible.

9. Conclusions

The transition time concept has been introduced for DCB specimens of different materials, proposing a time-based threshold criterion to define when the inertia effects can be neglected and a quasi-static data reduction method can be used. Three different methods to determine the transition time for the DCB test have been proposed: an analytical approach, a numerically-based approach and a graphical method. A dimensional analysis has been carried out using the Buckingham Pi theorem to obtain the numerically-based expression. Additionally, a geometrical scalability study has been performed to validate the use of the graphical method and the numerically-based approach. The numerically-based expression has proved to be a powerful tool to determine the transition time, resulting in smaller differences with respect to the FE simulation in comparison to the analytical expression.

The effect of the velocity profile and its maximum value on the dynamical response of the system has been also analysed, showing the importance of the dimensionless parameter D. The transition time has been proved to be independent of the maximum velocity

applied when $D = 2$ and up to a certain value when $D = 1$. However, the velocity profile will limit the use of the quasi-static analysis for higher maximum velocity values, especially when a step acceleration or close similar loading is applied ($D = 1$).

Thanks to the scalability analysis and the results of the velocity profile and its maximum value, the graphical method has proved to be useful to define an energy ratio curve for a particular DCB specimen. The obtained curve can be extrapolated to different DCB specimen configurations, geometries and materials, provided that the π-parameters π_2 and π_3 are kept constant.

The proportionality of the time-based threshold criterion has been defined based on the limit of energy ratio of 20% as t_f at least 2.03 times larger than t_τ. The results show that the proposed approach to determine the transition time and the use of the time-based threshold criterion might be useful tools to define when a quasi-static data-reduction scheme can be applied to calculate the mode I fracture toughness in symmetrical opening DCB tests under high loading rates. It is worth mentioning that the analysis is restricted to bending profiles assumed by quasi-static beam theory for the analytical approach. However, when using the numerically-based approach, the non-linear simulations already account for the bending profiles affected by the loading rates.

Declaration of competing interest

The authors declare that they have no known competing financial interests or personal relationships that could have appeared to influence the work reported in this paper.

Acknowledgements

The authors would like to acknowledge the financial support from the Spanish Ministerio de Ciencia, Innovación y Universidades through the projects RTI2018-099373-B-I00, RTI2018-097880-B-I00 and RTI2018-094435-B-C32. The first author also acknowledges the grant for doctoral studies IFUdG2017/43.

Appendix A. Preliminary dimensional analysis

In order to select the variables that affect the problem of the transition time in a DCB test under high loading rates, a preliminary dimensional study is carried out. Here, all the possible variables involved in the problem are considered, studying their effects and thereby choosing the critical ones for the reduced analysis of Section 5.2. The initial π-variables selected can be described as:

$$\frac{U_k}{U_e} = f\left(\delta, t, \dot{\delta}, c_o, a_o, h, b, l\right) \tag{A.1}$$

where U_k/U_e is the dependent variable, while δ and t are selected as the repeatable variables in order to obtain a π-parameter equivalent to the dimensionless displacement coefficient D introduced by Nakamura et al. [14] (see Eq. (13)).

According to the Buckingham Pi theorem, the relation can be described as follows:

$$\frac{U_k}{U_e} = f\left(\pi_{1p} = \frac{tc_o}{\delta}, \pi_{2p} = \frac{t\dot{\delta}}{\delta}, \pi_{3p} = \frac{a_o}{\delta}, \pi_{4p} = \frac{h}{\delta}, \pi_{5p} = \frac{b}{\delta}, \pi_{6p} = \frac{l}{\delta}\right) \tag{A.2}$$

To analyse the effect of each preliminary π-parameter, different FE simulations are carried out using the FE model described in Section 5.1. For the parametric study, the geometrical reference values for the models are: $l = 200$ mm, $b = 20$ mm, $h = 1.5$ mm and $a_o = 50$ mm. The material used in the study is Hexply AS4/8552 CFRP, whose properties are listed in Table 2. Besides, a linear acceleration ($D = 2$) is considered with a maximum velocity of 2 m/s for a time of 0.5 ms.

The parametric study is carried out by varying the variables that define the π-parameters according to the ranges and increments defined in Table A.1. It is worth noting that while one of the π-parameters is varied, the rest of the π-parameters remain constant. The variable c_o accounts for the change of the material properties, while the dimensionless parameter D takes the effect of the velocity.

Fig. A.1 shows the results of the preliminary parametric study. As it can be observed, there is no effect of the π_{6p}-parameter, that accounts for the length of the specimen (see Fig. A.1f). Besides, the effect of the π_{5p}-parameter, that accounts for the specimen width, is negligible, as it can be seen in Fig. A.1e. Accordingly, it is possible to discard these variables from the reduced dimensional analysis reported in Section 5.2. On the other hand, the rest of variables have an effect on the energy ratio and hence they are retained for the reduced dimensional analysis.

An additional remark is that when using the displacement δ as a repeating variable, it is not possible to vary the π_{1p}-parameter for a given material without varying t and δ and, thus, also vary parameter π_{2p}, which also depends on t and δ. This would require several simulations to obtain the curve of energy ratio. However, when using the crack length as repeating variable, it is possible to obtain the energy ratio curve with the information of only one FE simulation through the change of t but keeping constant a_o and the ratio t/δ. This is why, for the reduced dimensional analysis reported in Section 5.2, the crack length is used as repeating variable instead of the displacement.

Table A.1
Range of variation of the variables for the different preliminary π-parameters.

π-parameter	Variable to modify	Min. value	Max. value	Increment
π_{1p}	c_o [m/s]	2000	14000	250
π_{2p}	$\dot{\delta}$ [m/s]	0.1	3	0.1
π_{3p}	a_o [mm]	20	110	3
π_{4p}	h [mm]	0.4	3	0.1
π_{5p}	b [mm]	10	40	1
π_{6p}	l [mm]	80	200	5

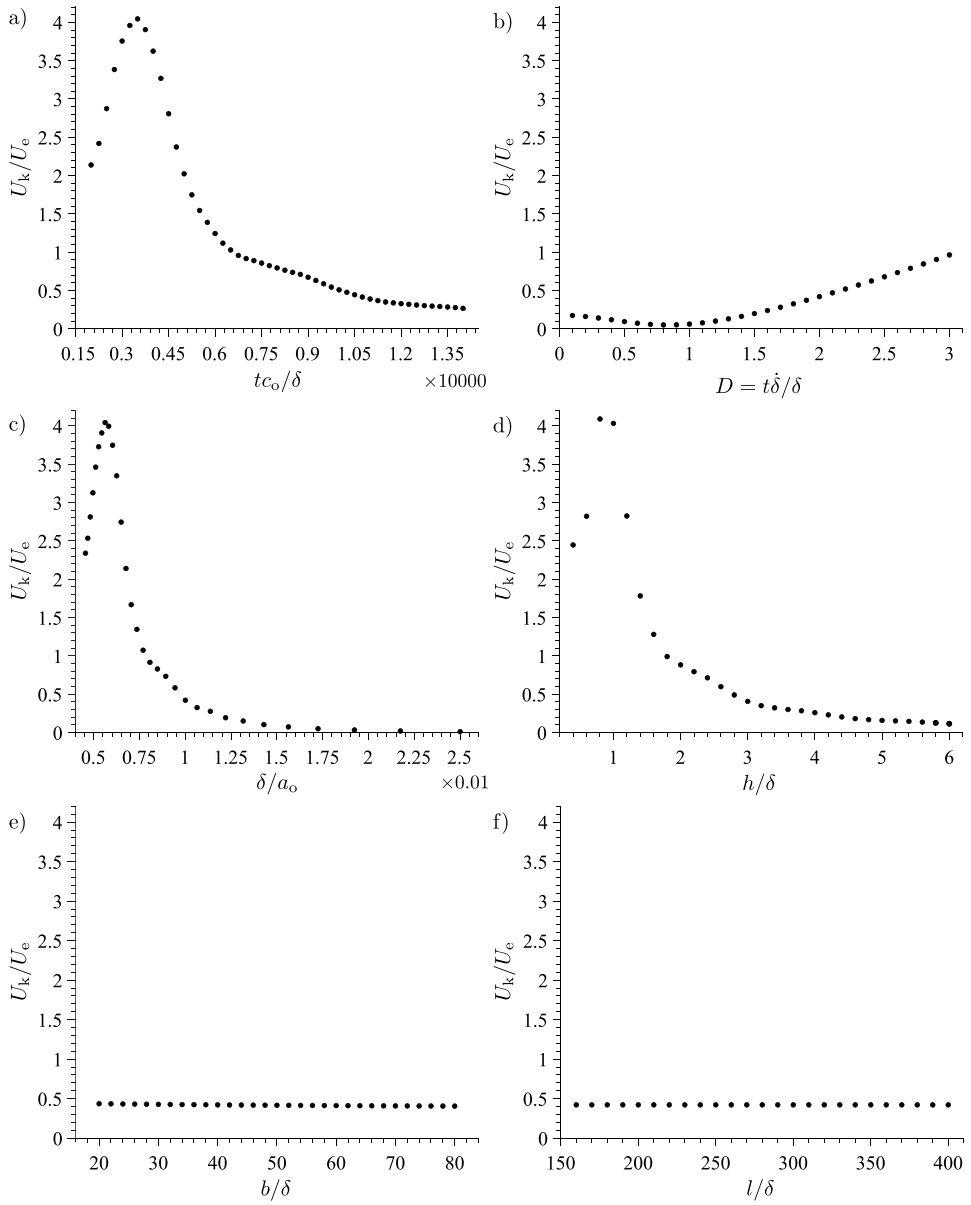

Fig. A.1. Curves of the energy ratio in terms of the preliminary π-parameters for (a) π_{1p}, (b) π_{2p}, (c) π_{3p}, (d) π_{4p}, (e) π_{5p} and (f) π_{6p}.

Appendix B. Fitting curves to obtain the numerically-based expression

This appendix shows the process to obtain a set of fitting expressions for the variation of the energy ratio versus each π-parameter considered in the reduced dimensional analysis of Section 5.2. For this parametric analysis, the results of the FE simulations for the

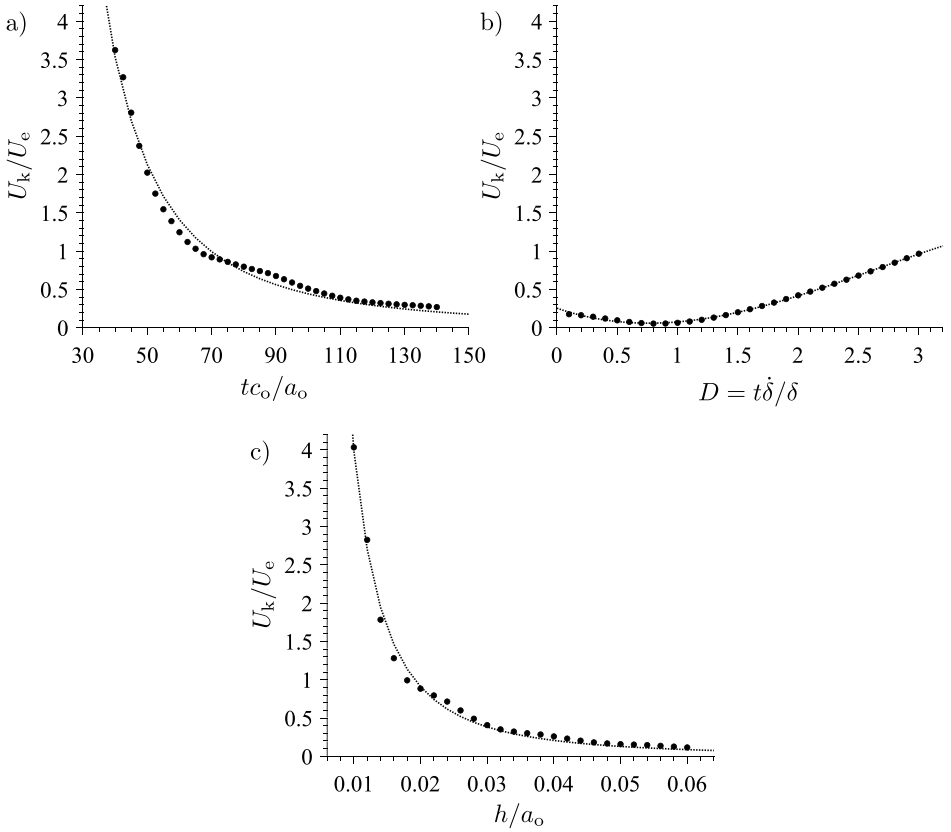

Fig. B.1. Fitting of the energy ratio curves in terms of the π-parameters for the reduced analysis (a) π_1, (b) π_2 and (c) π_3.

variables c_o, D and h from Appendix A are used. In order to obtain the energy ratio curves, the variables are set to the dimensionless form of the particular π-parameter associated, knowing that a_o and t are the repeating variables.

First, an expression that defines the complete variation of the energy ratio is adjusted using the least squares regression method for each π-parameter according to the curves of Fig. B.1. The fitting analysis describes the full behaviour of the π-parameters curves, which means including the initial stage of growth of the energy ratio where the kinetic energy is increasing in the system. The expressions obtained for each π-parameter can be expressed as:

$$\begin{aligned} &\text{for } \pi_1: \quad \frac{U_k}{U_e} = \frac{\pi_1}{(42.9244 - 2.362\pi_1 + 0.0395{\pi_1}^2)} \\ &\text{for } \pi_2: \quad \frac{U_k}{U_e} = 0.253792 - 0.543916\pi_2 + 0.417791{\pi_2}^2 - 0.052619{\pi_2}^3 \\ &\text{for } \pi_3: \quad \frac{U_k}{U_e} = \frac{1}{(0.8867 - 145.8592\pi_3 + 8345.633{\pi_3}^2)} \end{aligned} \tag{B.1}$$

With these expressions, the equation that describes the behaviour of the energy ratio is obtained as the product of the expressions of Eq. (B.1) for the π-parameters. The resulting expression for the energy ratio is:

$$\frac{U_k}{U_e} = 0.0525 \left(\frac{\psi}{\xi}\right) {a_o}^3 c_o t \tag{B.2}$$

where ψ is a polynomial function that accounts for the effects of the dimensionless parameter D and it is described as follows:

$$\psi = -0.3876D^3 + 3.0778D^2 - 4.0069D + 1.8696 \tag{B.3}$$

On the other hand, ξ is a function that accounts for the interaction of a_o, h, c_o and t. The function can be expressed as follows:

$$\xi = \left(\lambda_1 {a_o}^2 + \lambda_2 a_o h + \lambda_3 h^2\right)\left(\lambda_4 {a_o}^2 + \lambda_5 a_o c_o t + \lambda_6 {c_o}^2 t^2\right) \tag{B.4}$$

where $\lambda_1 = 0.076$; $\lambda_2 = -12.529$; $\lambda_3 = 716.884$; $\lambda_4 = 193.314$; $\lambda_5 = -10.638$ and $\lambda_6 = 0.178$.

The use of Eq. (B.2) to obtain the transition time derives in a complex solution, being impractical to use. For this reason, a new fitting analysis is carried out only taking into account the part of the curves relevant for the determination of the transition time,

i.e. once the energy ratio starts to decrease, as shown in Fig. B.1. Following the same procedure as for the full behaviour of the energy ratio, the fitting expressions adjusted using the least squares regression method are:

$$\begin{aligned} \text{for } \pi_1: \quad & \frac{U_k}{U_e} = 1.5237 \times 10^4 {\pi_1}^{-2.269} \\ \text{for } \pi_2: \quad & \frac{U_k}{U_e} = -0.0526{\pi_2}^3 + 0.4178{\pi_2}^2 - 0.5439\pi_2 + 0.2538 \\ \text{for } \pi_3: \quad & \frac{U_k}{U_e} = 2.1632 \times 10^{-4} {\pi_3}^{-2.133} \end{aligned} \tag{B.5}$$

The equation that describes the behaviour of the energy ratio is obtained once again as the product of the π-parameters. From this analysis, a new expression that involves the DCB test parameters can be obtained as:

$$\frac{U_k}{U_e} = \psi \frac{a_o^{4.402}}{c_o^{2.269}\ h^{2.133}\ t^{2.269}} \tag{B.6}$$

References

[1] Soutis C. Fibre reinforced composites in aircraft construction. Prog Aerosp Sci 2005;41(2):143–51. http://dx.doi.org/10.1016/j.paerosci.2005.02.004.

[2] ISO 15024:2001. Fibre-reinforced plastic composites — Determination of mode I interlaminar fracture toughness, GIC, for unidirectionally reinforced materials. Standard, Geneva, CH: International Standardization Organization; 2001, p. 24.

[3] Cantwell WJ, Blyton M. Influence of loading rate on the interlaminar fracture properties of high performance composites - A review. Appl Mech Rev 1999;52(6):199. http://dx.doi.org/10.1115/1.3098934.

[4] Jacob GC, Starbuck JM, Fellers JF, Simunovic S, Boeman RG. The effect of loading rate on the fracture toughness of fiber reinforced polymer composites. J Appl Polym Sci 2005;96(3):899–904. http://dx.doi.org/10.1002/app.21535.

[5] May M. Measuring the rate-dependent mode I fracture toughness of composites – A review. Composites A 2016;81:1–12. http://dx.doi.org/10.1016/J.COMPOSITESA.2015.10.033.

[6] Jiang F, Vecchio KS. Hopkinson bar loaded fracture experimental technique: A critical review of dynamic fracture toughness tests. Appl Mech Rev 2009;62(6):060802. http://dx.doi.org/10.1115/1.3124647.

[7] Blackman BRK, Dear JP, Kinloch AJ, Macgillivray H, Wang Y, Williams JG, Yayla P. The failure of fibre composites and adhesively bonded fibre composites under high rates of test. Part I Mode I loading - experimental studies. J Mater Sci 1995;30(23):5885–900. http://dx.doi.org/10.1007/BF01151502.

[8] Blackman BRK, Kinloch AJ, Rodriguez Sanchez FS, Teo WS, Williams JG. The fracture behaviour of structural adhesives under high rates of testing. Eng Fract Mech 2009;76(18):2868–89. http://dx.doi.org/10.1016/j.engfracmech.2009.07.013.

[9] Colin de Verdiere M, Skordos AA, May M, Walton AC. Influence of loading rate on the delamination response of untufted and tufted carbon epoxy non crimp fabric composites: Mode I. Eng Fract Mech 2012;96:11–25. http://dx.doi.org/10.1016/j.engfracmech.2012.05.015.

[10] Anderson TL. Fracture mechanics: fundamentals and applications. Boca Raton, FL: CRC Press; 2005, p. 610.

[11] Kalthoff JF, Beinert J, Winkler S. Measurements of dynamic stress intensity factors for fast running and arresting cracks in double-cantilever-beam specimens. In: Fast fracture and crack arrest. 100 Barr Harbor Drive, PO Box C700, West Conshohocken, PA 19428-2959: ASTM International; 1977, p. 161–161–16. http://dx.doi.org/10.1520/STP27387S.

[12] Chen T, Harvey CM, Wang S, Silberschmidt VV. Dynamic interfacial fracture of a double cantilever beam. Eng Fract Mech 2020;225:106246. http://dx.doi.org/10.1016/j.engfracmech.2018.11.033.

[13] Chen T, Harvey CM, Wang S, Silberschmidt VV. Delamination propagation under high loading rate. Compos Struct 2020;253:112734. http://dx.doi.org/10.1016/j.compstruct.2020.112734.

[14] Nakamura T, Shih CF, Freund LB. Analysis of a dynamically loaded three-point-bend ductile fracture specimen. Eng Fract Mech 1986;25(3):323–39. http://dx.doi.org/10.1016/0013-7944(86)90129-3.

[15] Nakamura T, Shih CF, Freund LB. Three-dimensional transient analysis of a dynamically loaded three-point-bend ductile fracture specimen. In: Nonlinear fracture mechanics: Volume I time-dependent fracture. 100 Barr Harbor Drive, PO Box C700, West Conshohocken, PA 19428-2959: ASTM International; 1989, p. 217–41. http://dx.doi.org/10.1520/STP26778S.

[16] ISO 12135:2016. Metallic materials – Unified method of test for the determination of quasistatic fracture toughness. Standard, Geneva, CH: International Standardization Organization; 2016, p. 98.

[17] ISO 12737:2010. Metallic Materials — Determination of plane-strain fracture toughness. Standard, Geneva, CH: International Standardization Organization; 2010, p. 18.

[18] ISO 148:2016. Metallic Materials — Charpy pendulum impact test — Part 1: Test method. Standard, Geneva, CH: International Standardization Organization; 2016, p. 29.

[19] Ireland DR. Critical review of instrumented impact testing. In: Dawes M, editor. International conference on dynamic fracture toughness. London, UK: The Welding Institute; 1976, p. 47–62.

[20] Böhme W. Dynamic key-curves for brittle fracture impact tests and establishment of a transition time. In: Fracture mechanics: Twenty-first symposium. 100 Barr Harbor Drive, PO Box C700, West Conshohocken, PA 19428-2959: ASTM International; 1990, p. 144–56. http://dx.doi.org/10.1520/STP18993S.

[21] McCarroll CA. High rate fracture toughness measurement of laminated composites [Ph.D. thesis], Imperial College London; 2011.

[22] Kalthoff JF. On the measurement of dynamic fracture toughnesses - a review of recent work. Int J Fract 1985;27(3–4):277–98. http://dx.doi.org/10.1007/BF00017973.

[23] Zehnder AT, Rosakis AJ. Dynamic fracture initiation and propagation in 4340 steel under impact loading. Int J Fract 1990;43(4):271–85. http://dx.doi.org/10.1007/BF00035087.

[24] Yokoyama T, Kishida K. A novel impact three-point bend test method for determining dynamic fracture-initiation toughness. Exp Mech 1989;29(2):188–94. http://dx.doi.org/10.1007/BF02321374.

[25] Sunny G, Prakash V, Lewandowski JJ. Dynamic fracture of a Zr-based bulk metallic glass. Metall Mater Trans A 2013;44(10):4644–53. http://dx.doi.org/10.1007/s11661-013-1810-z.

[26] Shazly M, Prakash V, Draper S. Dynamic fracture initiation toughness of a gamma (met-PX) titanium aluminide at elevated temperatures. Metall Mater Trans A 2009;40(6):1400–12. http://dx.doi.org/10.1007/s11661-009-9823-3.

[27] Martins CF, Irfan MA, Prakash V. Dynamic fracture of linear medium density polyethylene under impact loading conditions. Mater Sci Eng A 2007;465(1–2):211–22. http://dx.doi.org/10.1016/J.MSEA.2007.02.010.

[28] Jones RL, Davies PC. Experimental characterisation of dynamic tensile and fracture toughness properties. Fatigue Fract Eng Mater Struct 1989;12(5):423–37. http://dx.doi.org/10.1111/j.1460-2695.1989.tb00550.x.

[29] ASTM E23-18. Standard test methods for notched bar impact testing of metallic materials. Standard, West Conshohocken, PA: ASTM International; 2018, p. 26. http://dx.doi.org/10.1520/E0023-18.
[30] Henschel S, Krüger L. Dynamic crack initiation measurements in a four-point split Hopkinson bending device. Eng Fract Mech 2015;133:62–75. http://dx.doi.org/10.1016/J.ENGFRACMECH.2015.05.020.
[31] Koppenhoefer KC, Dodds RH. Constraint effects on fracture toughness of impact-loaded, precracked Charpy specimens. Nucl Eng Des 1996;162(2–3):145–58. http://dx.doi.org/10.1016/0029-5493(95)01151-X.
[32] Takashima Y, Minami F. Influence of impact velocity on transition time for V-notched Charpy specimen. Q J Japan Weld Soc 2017;35(2):80s–4s. http://dx.doi.org/10.2207/qjjws.35.80s.
[33] Dutton AG, Mines RAW. Analysis of the Hopkinson Pressure Bar loaded Instrumented Charpy Test using an inertial modelling technique. Int J Fract 1991;51(3):187–206. http://dx.doi.org/10.1007/bf00045806.
[34] Dassault Systèmes Simulia Corp. Abaqus analysis user's manual. In: Abaqus Documentation 6.14. Providence, RI, USA: Simulia Worldwide Headquarters; 2014.
[35] Buckingham E. On physically similar systems; illustrations of the use of dimensional equations. Phys Rev 1914;4:345–76. http://dx.doi.org/10.1103/PhysRev.4.345.
[36] Hug G, Thévenet P, Fitoussi J, Baptiste D. Effect of the loading rate on mode I interlaminar fracture toughness of laminated composites. Eng Fract Mech 2006;73(16):2456–62. http://dx.doi.org/10.1016/J.ENGFRACMECH.2006.05.019.
[37] Blackman BRK, Kinloch AJ, Wang Y, Williams JG. The failure of fibre composites and adhesively bonded fibre composites under high rates of test. Part II Mode I loading - dynamic effects. J Mater Sci 1996;31(17):4451–66. http://dx.doi.org/10.1007/BF00366341.
[38] Soto A, González EV, Maimí P, Mayugo JA, Pasquali PR, Camanho PP. A methodology to simulate low velocity impact and compression after impact in large composite stiffened panels. Compos Struct 2018;204:223–38. http://dx.doi.org/10.1016/J.COMPSTRUCT.2018.07.081.
[39] Soto A, González EV, Maimí P, Martín de la Escalera F, Sainz de Aja JR, Alvarez E. Low velocity impact and compression after impact simulation of thin ply laminates. Composites A 2018;109:413–27. http://dx.doi.org/10.1016/J.COMPOSITESA.2018.03.017.
[40] Benzeggagh ML, Kenane M. Measurement of mixed-mode delamination fracture toughness of unidirectional glass/epoxy composites with mixed-mode bending apparatus. Compos Sci Technol 1996;56(4):439–49. http://dx.doi.org/10.1016/0266-3538(96)00005-X.
[41] Soto A, González EV, Maimí P, Turon A, Sainz de Aja JR, Martín de la Escalera F. Cohesive zone length of orthotropic materials undergoing delamination. Eng Fract Mech 2016;159:174–88. http://dx.doi.org/10.1016/J.ENGFRACMECH.2016.03.033.
[42] ASTM D5528-13. Standard test method for mode I interlaminar fracture toughness of unidirectional fiber-reinforced polymer matrix composites. Standard, West Conshohocken, PA: ASTM International; 2013, p. 13. http://dx.doi.org/10.1520/D5528-13.